# Exploring Improvement in PMSM Drive Performance and Reliability Enabled by Futuristic Power Electronics

Alastair P. Thurlbeck*, *Student Member, IEEE,* Derek Jackson*, *Student Member, IEEE,* Vinson Guov*, *Student Member, IEEE,* Yue Cao, *Member, IEEE*

**Abstract**: As power semiconductor technologies continue to improve, futuristic switching devices, as projected to 10-20 years ahead, with ultra-low-cost and nearly-ideal behaviors (e.g., highly-efficient, minimal impedance imbalance, highly-reliable, etc.), will enable the use of increasingly complex power electronic systems. Currently the design of a permanent magnet synchronous motor drive is partially constrained by the inverter, since the use of more switches incurs additional cost and control complexity, and reduces efficiency. Assuming next-generation semiconductors will enable the use of many switches in the inverter with little penalty, this forward-looking paper considers the use of multilevel inverters with any number of levels, multiphase drives with higher numbers of phases, or a motor with reconfigurable windings, with the objective of opening up the operating space of a motor drive. In addition to exploring the performance benefits to the permanent magnet synchronous motor drive system, we highlight the improved fault-tolerance and therefore reliability of these more complex topologies compared to the conventional two-level three-phase system.

***Index Terms*—Permanent magnet synchronous motor drives, inverters, future technology, low-cost power electronics, ideal power semiconductors, multi-level inverters, multi-phase permanent magnet synchronous motor, reconfigurable permanent magnet synchronous motor windings, fault-tolerance, reliability.**

## I. Introduction

In this work we consider the impact of ultra-low-cost, nearly-ideal (e.g., highly-efficient, minimal impedance imbalance, highly-reliable, etc.), next generation switching devices on permanent magnet synchronous motor (PMSM) drives. If a switching device has minimal cost relative to the rest of the system, and its efficiency is exceptionally high, then adopting complex drive topologies with very large numbers of switches becomes viable. We consider a futuristic scenario, as projected to 10-20 years ahead, in which the power electronic switching devices and their associated gate drivers are nearly lossless and free, and the controller can control an arbitrarily large number of PWM outputs. Whilst unrealistic, this enables us to explore possible performance and reliability improvements to the motor drive, when its design is unconstrained by the quantity of switching devices and the complexity of the associated control system. In doing so, we explore possible future motor drive configurations which offer improved performance or reliability compared to conventional drives and have the potential to be practical in the long-term as future power electronic technologies are developed.

With no constraint on the number of switches, more complex inverter topologies offer benefits over the traditional three-phase two-level inverter. Firstly, fault-tolerance and reliability can be improved through the use of a fault-tolerant topology. Fault-tolerance can be added to a three-phase PMSM drive by a fourth inverter leg connected to the motor neutral, or acting as a direct replacement for a faulted phase leg [1]. A three-level active neutral point clamped (ANPC) inverter is well suited to fault-tolerant operation, since the additional switches provide an inherent capability to isolate faults [2]. Similarly, a cascaded H-Bridge (CHB) multi-level inverter (MLI) lends itself to fault-tolerant operation, since a faulty H-bridge cell can be bypassed and compensated for by a fault-tolerant control technique [3]. A five-year industrial application test demonstrated the improved reliability of a fault-tolerant MLI in [4]. Fault-tolerance is also enabled by PMSMs with more than three windings. A dual-winding PMSM with two 3-phase inverters offers fault-tolerance to both PMSM and inverter faults [5]. Multiphase PMSMs with five phases or more offer improved fault-tolerance compared to a three phase PMSM. This is because the amount of additional current required in the remaining phases to maintain torque production is reduced as the phase number increases. 5-phase PMSMs are already common in safety-critical applications, where each phase can be driven by an independent H-bridge drive unit for improved resiliency [6].

Beyond improving fault-tolerance, additional switches can also realize performance improvements to the PMSM drive system. A multiphase PMSM with concentrated windings can achieve higher torque density, with the increased improvement with the number of phases [7], [8]. The PMSM is designed such that the back EMF waveforms contain the odd-numbered harmonics with orders less than the number of phases in the machine. Then by harmonic current injection, torque is produced by the lower order harmonics in addition to the fundamental, allowing for improved torque-density.

A PMSM with reconfigurable windings can also improve performance, especially in applications requiring a

This work was supported in part by the Grainger Center for Electric Machinery and Electromechanics at the University of Illinois.

A. P. Thurlbeck, D. Jackson, V. Guov, and Y. Cao are with the School of Electrical Engineering and Computer Science, Oregon State University, Corvallis, OR 97331, USA. e-mail: thurlbea@oregonstate.edu, jacksder@oregonstate.edu, guovv@oregonstate.edu, yue.cao@oregonstate.edu

(*) Alastair P. Thurlbeck, Derek Jackson, and Vinson Guov are co-first authors with equal contributions to this work.

wide range of speeds such as electric vehicles. Reconfigurable windings is enabled by power electronics switching, allowing fast winding changeover during operation with minimal interruption. Field-weakening has traditionally been employed to increase maximum speed, but sacrifices machine efficiency as the field-weakening currents increase with speed. Reconfigurable windings provide an alternative, enabling higher speeds without field-weakening. This is demonstrated in [9], with a five-phase PMSM and 15 switches to achieve winding changeover between three different winding configurations (star, pentagon, pentacle) during operation. Ref [10] uses a different approach, with each phase divided into several winding parts instead of rearranging the connections between phases as in [9]. By eliminating the need to produce field-weakening currents, efficiency is improved at high speed [11]. Lastly, the MLI can reduce phase current total harmonic distortion (THD) and torque ripple without increasing the switching frequency [12]. Introducing multiple voltage levels can also reduce dv/dt (for the same voltage output) and offer higher reliability compared to their 2 or 3-level counterparts [13]. Despite these advantages, the use of fault-tolerant drives, high phase numbers, reconfigurable windings, and MLIs remains limited due to the high component count, with additional power semiconductor switches incurring additional cost and losses.

As future power electronics diminishes the drawbacks of additional switching devices, these more complex drive topologies will become attractive in a wider range of applications. Considering our ideal hypothetical case, in which the switching devices are free and lossless, it is clear any of the aforementioned fault-tolerant strategies could be employed with minimal penalty. However, for the multiphase and multilevel inverters, there is a question of how many phases or how many levels are adequate to achieve a desired reliability or performance improvement. In this paper, we therefore focus on exploring the benefits to fault-tolerance and drive performance in three scenarios: 1) a multiphase PMSM drive with a high number of phases; 2) a CHB MLI with a high number of levels; 3) a PMSM with reconfigurable phase windings.

Section II uses a simulation study of fault-tolerant multiphase PMSMs to investigate the post-fault torque ripple and normalized winding loss as the number of phases is increased. In Section III, two possible scaling methods for multiphase PMSMs are explored, assuming the copper mass should be kept constant as the number of phases increases. Section IV evaluates the reliability improvement offered by a fault-tolerant CHB MLI as the number of levels is increased. Following in Section V, the torque ripple and phase current THD of the CHB MLI is investigated in the healthy and post-fault operating conditions. Then in Section VI, the efficiency gain from a PMSM with reconfigurable windings is evaluated.

## II. Fault-tolerance of Multiphase PMSMs

PLECS modeling software is used to simulate the healthy and post-fault operation of multiphase motor drives. We assume a fault results in the loss of one phase, leaving $n$-1 operational phases in an $n$-phase machine. Two post-fault strategies are considered. In the first strategy, the remaining phase currents are increased in magnitude to compensate for the loss of a single phase. However, their phases are unaltered and the space vector trajectory of the current becomes non-circular, resulting in torque ripple. In the second strategy, the objective is to minimize torque ripple. By varying both the magnitude and phase of the remaining phase currents, a circular space vector trajectory and therefore zero torque ripple can be achieved [14]. Fig. 1 shows the post-fault torque ripple and the post-fault winding loss normalized to healthy operation under each post-fault strategy.

From the simulated data and Fig. 1, we observe that torque ripple and normalized winding loss adhere to the following relationship for the post-fault, minimized winding loss strategy:

$$\Delta T_{em(pk-pk)} = \frac{2}{n-2} \tag{1}$$

$$P_{loss\_windings} = 1 + \frac{1}{n-2} \tag{2}$$

where $n$ is the number of phases in the healthy PMSM and $n$-1 phases are operational post-fault. As expected, torque ripple tends to zero as the number of phases increases, whilst the normalized power loss tends to one. Considering the post-fault, minimized torque ripple-case, the ideal simulation results in zero torque ripple for any phase number greater or equal to five. A neutral connection would be required to achieve zero-torque ripple in a post-fault three-phase machine, and is not considered here. For a given phase number, normalized winding loss is higher in the minimized torque ripple strategy, however this loss is

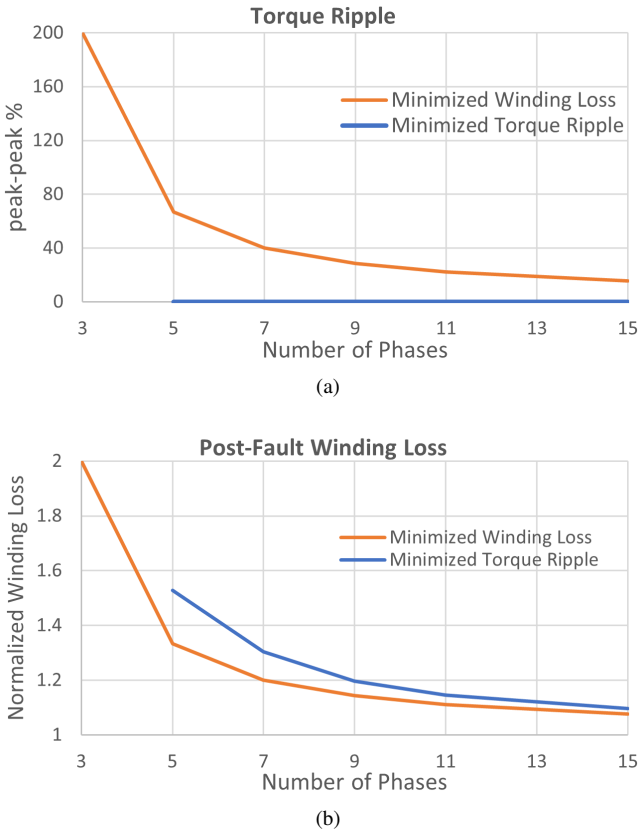


Fig. 1. Post-fault performance following the loss of one phase under two possible post-fault strategies: minimized winding loss, and minimized torque ripple. (a) Electromagnetic torque ripple. (b) Normalized winding loss.

equally distributed among the windings due to the balanced phase currents.

As Fig. 1 shows, there is a dramatic improvement in post-fault performance in moving from 3 to 5 phases. Considering the minimized winding loss case, using (1) and (2) we can find the required number of phases for a required torque ripple or winding loss specification. For post fault torque ripple within $\pm 10\%$ and post-fault winding loss within 10% of the healthy condition, 13 phases are required. Beyond this point, returns diminish rapidly, with 5% requiring 23 phases, and 1% requiring 103. At these higher phase numbers, machine design constraints would become a limiting factor. Future safety-critical PMSM drives may see a shift from the typical 3 or 5 phases to higher phase numbers, as the future power electronics enables high switch count inverters to be used with minimal cost and efficiency penalty.

## III. Relative Performance of Multiphase Machines

Multiphase PMSMs have been demonstrated to offer a torque density improvement, when designed with concentrated windings and used with the harmonic current injection technique [7], [8], [15]. Here we consider only the sinusodially distributed winding case, which is not expected to offer a torque density improvement. Still, higher phase numbers in a sinusoidally wound PMSM may be desirable to improve post-fault performance, as discussed in the previous section. Therefore, this section intends to investigate the effect of increasing phase numbers on phase current THD and efficiency. Assuming that the total volume and mass of copper in the PMSM must be kept constant across all phase numbers, other PMSM parameters must be appropriately scaled as the number of phases increases. We consider two possible scaling methods. In the **first scaling method**, cross-sectional winding area is inversely proportional to the number of phases, and the length and number of turns in each winding is unchanged. The stator inductance and the rotor flux linkage are constant, whilst stator resistance is calculated as $R_{s(n)} = (n/3)R_{s(3)}$, where $R_{s(3)}$ is the stator resistance of the baseline 3-phase PMSM. In the **second scaling method**, cross sectional area is constant, and now the length and number of turns in each winding is inversely proportional to the number of phases. Therefore, stator resistance, stator inductance, and rotor flux linkage all vary with the number of phases as follows:

$$R_{s(n)} = \frac{3}{n}R_{s(3)} \quad L_{s(n)} = \frac{3}{n}L_{s(3)} \quad \lambda_{fd(n)} = \frac{3}{n}\lambda_{fd(3)} \tag{3}$$

where $L_{s(3)}$ and $\lambda_{fd(3)}$ are the stator inductance and the rotor flux linkage of the baseline three-phase machine. Leakage inductance is assumed to be 40% of the stator inductance in each motor.

Each scaling method was simulated for 3, 5, 7, and 9 phase PMSMs. The load torque was set to 10 Nm, and the commanded speed was 100 rad/s. Each inverter uses carrier based pulse width modulation, with a switching frequency of 50 kHz, and a deadtime of 1 $\mu$s. Fig. 2 shows the RMS phase current, phase current THD, and PMSM efficiency for each motor. For efficiency, only the effect of winding conduction losses is considered. The observed difference

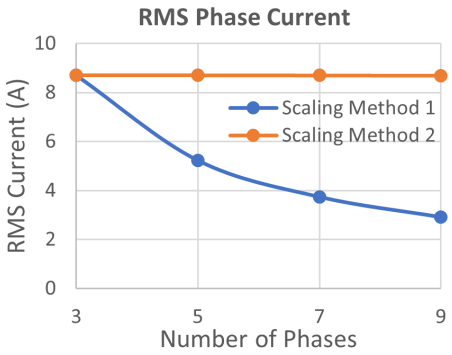


(a)

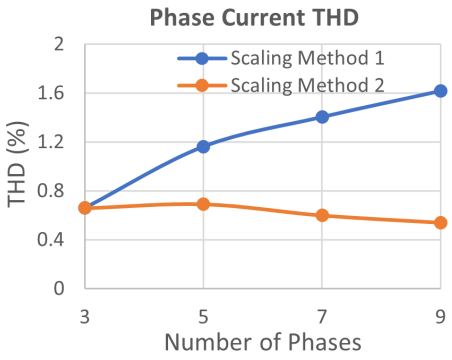


(b)

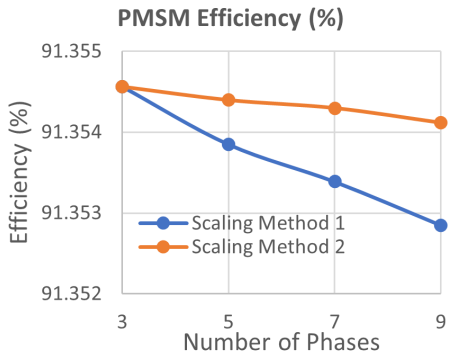


(c)

Fig. 2. PMSM drive performance under two possible scaling methods. (a) RMS phase current. (b) Phase current THD. (c) PMSM efficiency considering only winding losses.

in phase current THD and losses is very small. However, for the first scaling method, in which the cross-sectional winding area is inversely proportional to the number of phases, increasing the number of phases results in increasing THD and reducing efficiency. This effect is driven by the phase current ripple due to the PWM switching. With this scaling method, the magnitude of an individual phase current is reduced as the number of phases are increased, yet the magnitude of the switching ripple is largely unchanged. Therefore, the ratio of the ripple to the fundamental current is increasing with the number of phases, and therefore THD is increased. This causes a very small reduction in efficiency.

## IV. Reliability of Multilevel Inverters

A cascaded H-bridge (CHB) 3-phase MLI with $n$ number of cells in each phase has $N = 2n + 1$ voltage levels. We simulate this MLI with increasing $n$-cells to investigate the performance and reliability improvements to

the PMSM drive, and determine the point at which further improvement becomes negligible. Indeed, more points of failure are introduced as a result of increasing the voltage levels and cell count. However, the overall drive reliability can be improved given proper design. Whether or not the MLI offers improved reliability depends on the number of faults it can handle. To maintain the same voltage space vector magnitude in post-fault operation, the non-faulted phase-legs voltage magnitudes must increase. How many faults the MLI can handle thus depends on the nominal DC bus voltage utilization. For example, if $100\%$ of $V_{DC}$ is required for operation, no post-fault control scheme can maintain this same output. If nominal operation uses $80\%$ of $V_{DC}$, there is sufficient bus voltage headroom for the non-faulted phase-legs voltage magnitudes to increase.

A CHB MLI can operate post-fault by removing the faulted cells with a bypass switch, where a neutral shift balances the phase currents post-fault by adjusting the two non-faulted phase-leg angles [3]. Whilst a fault can occur on any phase, we assume the MLI is reconfigured so all faulted cells are on phase A. With the neutral shift fault operation from [3], the maximum normalized output voltage is:

$$\hat{V} = \frac{r}{2n} + \frac{cos(\alpha - \frac{5\pi}{6})}{\sqrt{3}} \tag{4}$$

where $r$ is the number of cells still functional in phase A, and $\alpha$ is the post-fault phase angle. Using (4) it is shown that a faulted MLI with $r = n/2$ is equivalent to a non-faulted balanced MLI with $V_{DC}$ reduced to $80.9\%$ of its original magnitude.

Compared to an individual cell reliability $R_c$ over a time interval $T_r$, an $n$-cell MLI that cannot tolerate any faults will have a reduced reliability of $R_c^{3n}$. In this analysis we define failure as the point at which the MLI can no longer operate at the desired voltage $\hat{V}$ due to the loss of too many cells. Therefore, when the MLI can tolerate $n-r$ faults the MLI reliability $R_{MLI}$ is given as [16]:

$$R_{MLI} = \sum_{i=r+2n}^{3n} \binom{3n}{i} R_c^i (1-R_c)^{3n-i} \tag{5}$$

where $\binom{3n}{i}$ is the binomial coefficient. Given a sufficiently high $R_c$ and low $r$, $R_{MLI}$ offers improved reliability. A closed-form equation of $r$ for a fixed number of cells $n$ and a minimum operating voltage $\hat{V}$ is derived from the $\alpha$ equation (see [3]) and (4),

$$r = \left\lceil n \cdot \frac{3\hat{V} - \sqrt{4 - 3\hat{V}^2}}{2} \right\rceil, \hat{V} \geq \frac{1}{\sqrt{3}} \tag{6}$$

where $\lceil \cdot \rceil$ is the ceiling function, as $r$ is discrete and must be rounded up.

There is an exponential trend in reliability as the amount of $n$-cells increase. For example, if $R_c = 99\%$ and $\hat{V} = 80\%$ then a MLI with 10-cells per phase has $60,000$ times smaller of a probability of failure (PoF$= 1 - R_{MLI}$) over $T_r$ than a 1-cell inverter, while a MLI with 2-cells has only 20 times smaller of a PoF. An operating point of $\hat{V} = 80\%$ is selected for reliability comparison as it is the maximum output of a 2-cell MLI with $n/2$ faults on phase A. Fig. 3 shows the PoF for multiple $R_c$'s, and demonstrates the need for level redundancy decreases as semiconductor reliability continues to improve. To achieve a similar PoF of a 10-cell

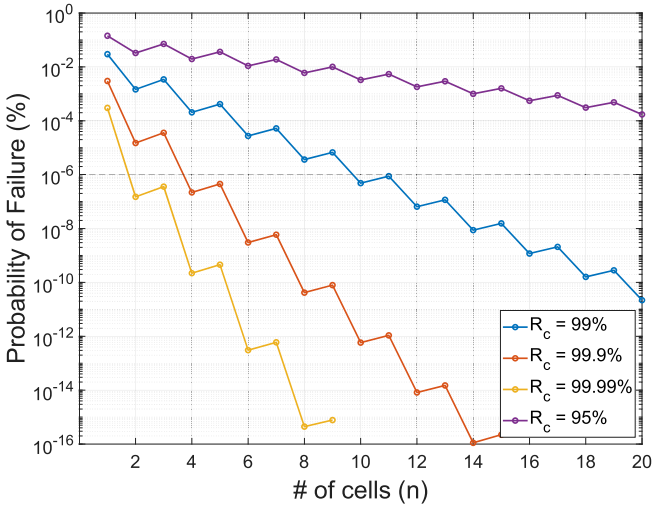


Fig. 3. Probability of failure (PoF) over time interval $T_r$ for multiple $R_c$'s, where $\hat{V} = 80\%$.

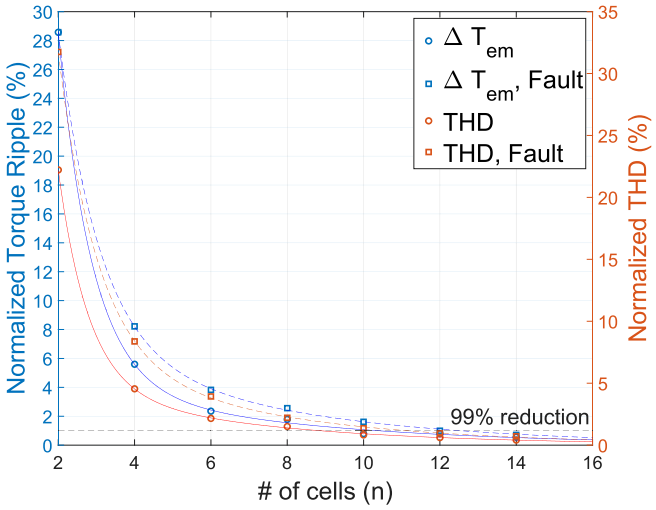


Fig. 4. Torque ripple and THD normalized by a 1-cell CHB MLI and an operating voltage of $\hat{V} = 80\%$.

MLI with $R_c = 99\%$, only 4-cells and 2-cells are needed when $R_c = 99.9\%$ and $R_c = 99.99\%$, respectively. The inverse is also true, where 38-cells are needed if $R_c = 95\%$. Note that the stair-case effect seen on the plot of Fig. 3 is caused by (6) with $\hat{V} = 80\%$ where $r = \lceil n/2 \rceil$.

## V. Motor Performance for $N$-Level Inverters

Section IV demonstrated the number of $N$-levels are unimportant for reliability concerns as semiconductor reliability increases. Thus, determining the $N$-levels of an inverter becomes dependent on its performance. Performance will be measured in terms of EM torque ripple $\Delta T_{em}$ and phase current THD. While minimum torque ripple and THD are entirely dependent on the application, this analysis will consider an inverter to be sufficient for an application when it achieves a $99\%$ reduction in torque ripple and THD compared to a single cell, 3-level CHB MLI. It should be noted that increasing switching frequency and utilizing advanced control and modulation techniques can also lower torque ripple. However, determining the number of levels where no discernable difference is seen by increasing the

levels is helpful in realizing saturation points in motor drive design, thereby ensuring minimum cost for performance.

PLECS was used to simulate and compare motor performance with varying $N$-levels of a CHB MLI, and phase-shifted sinusoidal PWM (PS-SPWM) modulation. Performance comparison uses the same operating point of Section IV, $\hat{V} = 80\%$ and load torque of $3.2\,Nm$. Each N-level inverter had a fault condition of $z = n/2$ faults. Note the probability for $z = n/2$ faults to occur decreases exponentially with respect to $n$. In this study, torque ripple is defined as $\Delta T_{em} = T_{pk-pk}/T_{avg}$. Fig. 4 is a plot of the normalized $\Delta T_{em}$ and THD. To achieve a $99\%$ reduction in $\Delta T_{em}$ requires a 10-cell CHB MLI. In fault condition, the 10-cell MLI still had a $98.5\%$ lower $\Delta T_{em}$ than the 1-cell inverter.

## VI. Efficiency Improvement from Reconfigurable Windings

Reconfigurable phase windings offer improved motor efficiency at high speeds and can be achieved by integrating switching devices within the phase windings. A surface permanent magnet (SPM) machine with its phase windings separated into two equal parts, shown in Fig. 5, is modeled in MATLAB to investigate the improvements. With two winding parts per phase, there are two configurations the machine can switch between. The first arrangement is to connect the two windings in series, and the second arrangement is to connect the two windings in parallel. This chosen implementation requires three switches per phase, or nine switches total.

For the machine model, we assume steady-state operation to calculate efficiency within its torque-speed capability. We also assume the machine does not saturate and only consider copper and mechanical losses. The following equations describe how the winding configurations affect the machine's phase inductance and permanent magnet flux linkage:

$$L = \frac{\mu N^2 A}{l} \tag{7}$$

$$\lambda = N\Phi \tag{8}$$

The inductance $L$ of a phase is proportional to its windings' $N$ turns squared. The permanent magnet flux linkage $\lambda$ of a phase is proportional to its windings' $N$ turns. Therefore, in the parallel configuration, the phase resistance and inductance is 1/4 of that of the serial winding configuration. The permanent magnet flux linkage in the parallel configuration is 1/2 of that of the serial winding configuration.

This means that at a given nonzero speed, the back-EMF generated in the parallel configuration is halved when compared to the serial configuration, which also halves torque capability for this non-salient machine. The different torque and speed capability for both configurations is shown in Fig. 6. The following equations were used to determine the efficiency of the machine [17]:

$$\eta = \frac{T_r \omega_r}{T_r \omega_r + 3R_s I_{ph,q}^2 + 3R_s I_{ph,d}^2 + B\omega_r} \tag{9}$$

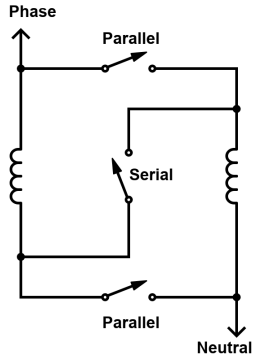


Fig. 5. Phase winding switch arrangement.

$$I_{ph,q} = \frac{T_r}{3k} \tag{10}$$

$$I_{ph,d} = I_{ph,m}\left(\frac{w_{r,rated}}{w_r} - 1\right) \tag{11}$$

$$I_{ph,m} = \frac{2k}{pL_s} \tag{12}$$

$\eta$ is the machine efficiency at a given rotor torque $T_r$ and rotor speed $\omega_r$. The copper losses are divided into d-axis current $I_{ph,d}$ and q-axis current $I_{ph,q}$. The machine's equivalent magnetizing current $I_{ph,m}$ can be calculated with the machine constant $k$ (Nm/A), pole count $p$, and stator inductance $L_s$. $I_{ph,d}$ is the field-weakening current, which is zero below rated speed and negative above rated speed.

In Fig. 7a, the efficiency is plotted against rotor torque and speed for the serial winding configuration. The region where efficiency is >94% occurs between approximately 1800 and 2800 RPM. As the speeds increase well above rated speed, the efficiency falls off due to the increasing field-weakening currents. In Fig. 7b, this is the scenario where the controller is continuously changing between the two winding configurations to operate at maximum efficiency. Since the parallel configuration has the advantage of less back-EMF, field-weakening is not required until the machine is above 5000 RPM as long as the required torque is within this configuration's capabilities, or 150 Nm in this case. Additionally, the parallel configuration has the benefit of reduced phase resistance, which further improves efficiency, assuming the winding switches are ideal. As a result, the high efficiency region (>94%) is expanded well above the original rated speed of the machine, now between approximately 1800 and 7800 RPM.

## VII. Conclusion

This paper investigated what benefits can be realized in a PMSM drive when unconstrained by switching devices. With the expectation that future switching devices may become ultra-low-cost and nearly ideal (e.g., highly-efficient, minimal impedance imbalance, highly-reliable, etc.), more complex topologies can be considered. Topologies such as multiphase drives with high phase numbers, a high number of levels in a multilevel inverter, or a PMSM with integrated switches to achieve reconfigurable windings may begin to offer a net improvement to the performance of the PMSM drive.

For a multiphase drive, scaling the length and turns in each winding was preferable to scaling the cross-sectional area of the wire. For multiphase fault-tolerance, 13 phases

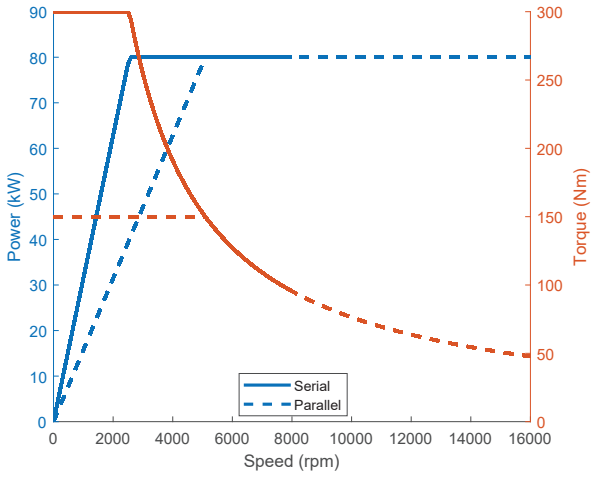


Fig. 6. Torque and power capability of serial/parallel winding configurations.

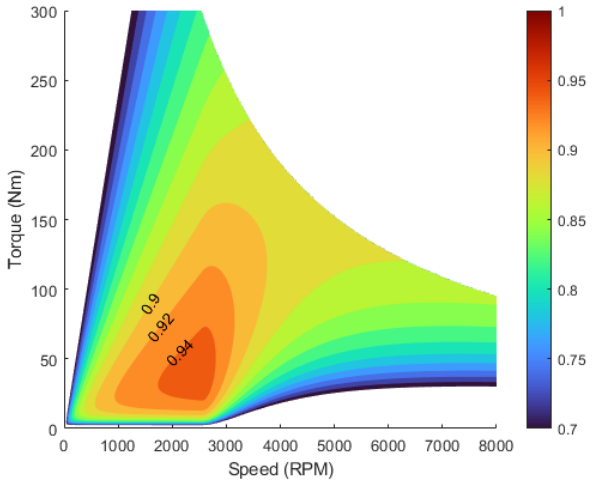


(a)

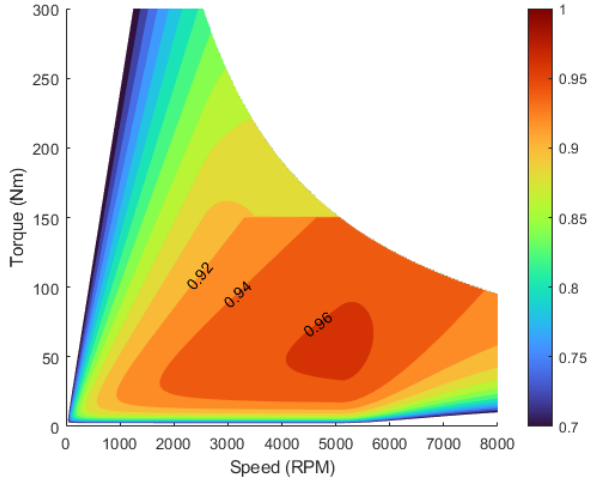


(b)

Fig. 7. (a) Serial winding machine efficiency map. (b) Combined serial/parallel machine efficiency map using adaptive switching.

was sufficient to reduce post-fault winding loss to within 10% of healthy operation, and torque ripple to within ±10%. If a minimized torque ripple strategy is used, 15 phases was sufficient to reduce post-fault winding loss to within 10% of healthy operation, and torque ripple is theoretically zero. Future switching devices can enable the use of a reconfigurable multilevel topology in which each cell may be bypassed or reallocated to another phase, allowing dramatic reliability improvements as the number of cells is increased. For the simulated operating conditions, a 6-cell (13-level) per phase inverter was shown to have a failure probability 1000 times lower than that of a 1-cell inverter. A saturation in performance occurs at 10-cells (21-level), with a 99% reduction in torque ripple compared to a 1-cell inverter. A motor with reconfigurable windings more than doubled the speed range for high efficiency (>94%) operation - from 1800-2800 RPM to 1800-7800 RPM. The reliance on field-weakening currents to achieve high speed was significantly reduced with the parallel winding configuration.

Future work will consider a more realistic MLI design in which cells may be bypassed, but cannot be reallocated between different phases. Then the MLI reliability analysis will be modified to consider failures occurring at random in all three phases. We will also consider the loss of more than one phase in a multiphase drive, and how this affects the reliability benefit offered by higher phase numbers. For reconfigurable windings, this concept could be applied to interior permanent magnet machines (IPMSM), which are highly applicable to electrified transportation.

## References


[1] B. Mirafzal, "Survey of fault-tolerance techniques for three-phase voltage source inverters," *IEEE Transactions on Industrial Electronics*, vol. 61, no. 10, pp. 5192–5202, 2014.

[2] J. Li, A. Q. Huang, Z. Liang, and S. Bhattacharya, "Analysis and design of active npc (anpc) inverters for fault-tolerant operation of high-power electrical drives," *IEEE Transactions on Power Electronics*, vol. 27, no. 2, pp. 519–533, 2012.

[3] J. Rodriguez, P. W. Hammond, J. Pontt, R. Musalem, P. Lezana, and M. J. Escobar, "Operation of a medium-voltage drive under faulty conditions," *IEEE Trans. Industrial Electronics*, vol. 52, no. 4, pp. 1080–1085, 2005.

[4] D. Eaton, J. Rama, and P. Hammond, "Neutral shift [five years of continuous operation with adjustable frequency drives]," *IEEE Industry Applications Magazine*, vol. 9, no. 6, pp. 40–49, 2003.

[5] X. Jiang, W. Huang, R. Cao, Z. Hao, and W. Jiang, "Electric drive system of dual-winding fault-tolerant permanent-magnet motor for aerospace applications," *IEEE Transactions on Industrial Electronics*, vol. 62, no. 12, pp. 7322–7330, 2015.

[6] B. C. Mecrow, A. G. Jack, J. A. Haylock, and J. Coles, "Fault tolerant permanent magnet machine drives," in *Proc. Seventh International Conference on Electrical Machines and Drives*, 1995, pp. 433–437.

[7] A. S. Abdel-Khalik, M. I. Masoud, S. Ahmed, and A. M. Massoud, "Effect of current harmonic injection on constant rotor volume multiphase induction machine stators: A comparative study," *IEEE Trans. Industry Applications*, vol. 48, no. 6, pp. 2002–2013, 2012.

[8] J. Wang, L. Zhou, and R. Qu, "Harmonic current effect on torque density of a multiphase permanent magnet machine," in *Proc. Int. Conf. Electrical Machines and Systems*, 2011, pp. 1–6.

[9] S. Sadeghi, L. Guo, H. A. Toliyat, and L. Parsa, "Wide operational speed range of five-phase permanent magnet machines by using different stator winding configurations," *IEEE Trans. Industrial Electronics*, vol. 59, no. 6, pp. 2621–2631, 2012.

[10] L. Tang, T. Burress, and J. Pries, "A reconfigurable-winding system for electric vehicle drive applications," in *Proc. IEEE Transportation Electrification Conference and Expo*, 2017, pp. 656–661.

[11] Y. Takatsuka, H. Hara, K. Yamada, A. Maemura, and T. Kume, "A wide speed range high efficiency ev drive system using winding changeover technique and sic devices," in *Proc. International Power Electronics Conference*, 2014, pp. 1898–1903.

[12] J. Rodriguez, J. -S. Lai, and F. Z. Peng, "Multilevel inverters: a survey of topologies, controls, and applications," *IEEE Trans. Industrial Electronics*, vol. 49, no. 4, pp. 724–738, 2002.

[13] S. Kouro, M. Malinowski, K. Gopakumar, J. Pou, L. G. Franquelo, B. Wu, J. Rodriguez, M. A. Pérez, and J. I. Leon, "Recent advances and industrial applications of multilevel converters," *IEEE Trans. Industrial Electronics*, vol. 57, no. 8, pp. 2553–2580, 2010.

[14] J. -R. Fu and T. A. Lipo, "Disturbance-free operation of a multiphase current-regulated motor drive with an opened phase," *IEEE Trans. Ind Appl.*, vol. 30, no. 5, pp. 1267–1274, 1994.

[15] H. -M. Ryu, J.-H. Kim, and S. -K. Sul, "Analysis of multiphase space vector pulse-width modulation based on multiple d-q spaces concept," *IEEE Trans. Power Electronics*, vol. 20, no. 6, pp. 1364–1371, 2005.

[16] P. Wikstrom, L. Terens, and H. Kobi, "Reliability, availability and maintainability (ram) of high power variable speed drive systems (vsds)," in *Proc. IEEE Industry Applications Society 45th Annu. Petroleum and Chemical Industry Conf.*, 1998, pp. 139–148.

[17] J. Hayes and G. Goodarzi, *Electric Powertrain: Energy Systems, Power Electronics and Drives for Hybrid, Electric and Fuel Cell Vehicles*. Hoboken, NJ: John Wiley & Sons Ltd, 2018, ch. 9.

## VIII. Biographies

**Alastair Thurlbeck** (Student Member, IEEE) received the M.Eng. degree (first class honors) in electronics and electrical engineering from the University of Glasgow, Glasgow, UK, in 2018.

Mr. Thurlbeck is currently a Ph.D. candidate at Oregon State University, Corvallis, OR, USA. He has been a Research Scientist Intern at Amazon Prime Air in Seattle, WA, USA; a Project Assistant with the University of Glasgow; a Hardware Intern with Curtis Instruments in Livermore, CA, USA; and a Summer Intern with Arqiva in Winchester, UK. His research interests include power electronics, motor drives, energy conversion, fault tolerance, and reliability.

Mr. Thurlbeck received the IEEE ITEC Conference Student Award in 2019. He was awarded the Gilbert Cook Prize in 2018, the William Dawson Bursary in 2015 and the Reid Foster prize in 2014 by the University of Glasgow. He was a recipient of the Diamond Jubilee Scholarship throughout his MEng degree, awarded by the Institute of Engineering and Technology (IET) in 2013.

**Derek Jackson** (Student Member, IEEE) received the B.S. and M.S. degrees in electrical and computer engineering with a minor in computer science from Oregon State University, Corvallis, OR, USA, in 2019 and 2021, respectively. Derek is currently pursuing a Ph.D. in electrical and computer engineering as part of the Energy Systems Group at Oregon State University.

As an undergraduate, he was an electrical engineering intern with the Product Validation Department at Daimler Trucks NA in Portland, OR, USA; and an electrical engineering intern with the Product Design Group at Blount International (now Oregon Tool) in Portland, OR, USA. His research interests include power electronics, motor drives, and power system design and optimization for transportation electrification and microgrids.

Derek received the IEEE ECCE Conference Student Travel Award for best student paper in 2020. He is vice-president of the IEEE Power & Energy Society (PES) and Power Electronics Society (PELS) Chapter at Oregon State University.

**Vinson Guov** (Student Member, IEEE) received his B.S. degree in Electrical and Computer Engineering from Oregon State University, Corvallis, OR, USA, in 2020. He is currently an M.S. student with the Energy Systems Group at Oregon State University.

Before completing his B.S. degree, Vinson was in the MECOP (Multiple Engineering Cooperative Program), completing two six-month internships at Vestas North America and Blount International (now Oregon Tool). Before joining the Energy Systems Group at OSU, Vinson completed a summer internship at Microchip in Bend, OR, to characterize SiC FETs. His research interests lie in electric vehicles, motor drives, power electronics, and renewable energy.

**Yue Cao** (Member, IEEE) received the B.S. degree (Hons.) in electrical engineering with a second major in mathematics from the University of Tennessee, Knoxville, TN, USA, in 2011, and the M.S. and Ph.D. degrees in electrical engineering from the University of Illinois at Urbana–Champaign (UIUC), Champaign, IL, USA, in 2013 and 2017, respectively.

Dr. Cao is currently an Assistant Professor with the Energy Systems Group at Oregon State University (OSU), Corvallis, OR, USA. Before joining OSU, he was a Research Scientist with the Propulsions Team at Amazon Prime Air in Seattle, WA, USA. He was a Power Electronics Engineer Intern with Special Projects Group at Apple Inc., Cupertino, CA, USA; Halliburton Company, Houston, TX, USA; Flanders Electric, Evansville, IN, USA; and Oak Ridge National Laboratory, TN, USA. He was a Sundaram Seshu Fellow in 2016 at UIUC, where he was a James M. Henderson Fellow in 2012. His research interests include power electronics, motor drives, and energy storage with applications in renewable energy integration and transportation electrification.

Dr. Cao received the Myron Zucker Award from the IEEE Industry Applications Society (IAS) in 2010. He was a recipient of Oregon State Learning Innovation Award for transformative education in 2020. He served as the Corresponding Technical Programs Chair of the 2016 IEEE Power and Energy Conference at Illinois (PECI). He is currently the Tutorials Chair of the 2021 IEEE Energy Conversion Congress Expo (ECCE) and the Special Sessions Chair of 2022 ECCE. He is a board member and Award Chair of IEEE Power Electronics Society (PELS) TC11 – Aerospace Power. In 2020, he helped establish an IEEE PELS Chapter at OSU. He is currently an Associate Editor for IEEE Transactions on Transportation Electrification.